# ENCLOSURE 1

# MFN 05-133

# Responses to DSS-CD TRACG LTR RAIs

Non-Proprietary Version

**IMPORTANT NOTICE**

This is a non-proprietary version of Enclosure 2, which has the proprietary information removed. Portions of the enclosure that have been removed are indicated by an open and closed bracket as shown here [[ ]]

## Table of Contents

**NRC RAI 1**

The TRACG case provided by GENE (PHE_10080_2PT_2TR_RENT_PLOT.INP) calculated the reactor response to a 2 recirculation pump trip transient. TRACG code predicted about 20% bypass void fraction in the upper part of the core during the transient prior to the instability. Please address the following questions regarding the bypass void fraction and its impact on the DSS-CD algorithm.

1.1 Please perform detailed calculations to provide accurate by-pass region axial void fraction profiles during the 2RPT transient.

1.2 Please provide the LPRM noise (amplitude and frequency) versus void fraction relationship.

1.3 Based on the noise level determined in 1.2, identify the operability of the LPRM at level A, B, C and D. Examine the impact of the noise on the LPRM/OPRM performance, DSS-CD confirmation counts, scram signal timing and CPR margin.

1.4 Zero by-pass voiding has been one of the fundamental assumptions of GE's TRACG transient analysis methodology. No by-pass void is assumed during the x-section generation process. The PANACEA code also has limited capability to model the by-pass void, i.e 1-D averaging approach. It is not clear how TRACG handles the by-pass void fraction. Therefore, with by-pass void, is the current GE reload methodology still valid? Please provide detailed discussion regarding how the by-pass void fraction is being modeled and examine the adequacy of the method to model the 2RPT transient. Please explain how the uncertainty of SLMCPR and CPR are evaluated when none-zero bypass void exists.

**GE Response**

Response to Part 1.1

The Perry two-pump trip TRACG case (PHE_10080_2PT_2TR_RENT_PLOT.INP) along the EPU/MELLLA+ boundary was re-performed with a detailed nodalization in the bypass region to investigate the bypass voiding phenomenon. [[

]]

Response to Part 1.2

The worst-case bypass voiding condition exists at natural circulation after trip of both recirculation pumps. At the end of this transient (flow ~30% and power ~60% of 120% uprate of highest power density BWR type MELLLA+ operation) the bypass voids at the D and C level LPRMs surrounded by four high power bundles could be [[ ]] which corresponds to a thermal neutron flux depression at these LPRM locations of [[ ]] The bypass region around A and B level LPRMs show negligible voiding, hence negligible flux depression during the event. The core wide average D and C level bypass voids at the end of the two pump trip transient are [[ ]]

The D and C level LPRM detectors may also indicate additional noise due to the void bubbles in the bypass region. The frequency of this noise is inversely related to the bubble transit time across the LPRM detector (~ 2 inches). For a typical bypass flow velocity at natural circulation of [[ ]] the noise frequency is [[ ]] This noise would have to be combined with the normal neutron noise at this location, to get the overall noise in the measured LPRM signal.

Response to Part 1.3

The current OPRM cell design contains no more than two D and two C level LPRMS, so based on a potential flux reduction of [[

]] the highest OPRM cell flux depression would be approximately 9% if all the detectors were at the same flux, and would generally be lower since the D level detectors see a lower flux than the A, B and C level detectors. Thus conservatively, bypass voids could attenuate the measured oscillation amplitude in an OPRM cell around the hottest bundles by [[ ]] at natural circulation following a 2 pump trip. This has insignificant effect on detecting the approach to the DSS-CD amplitude discriminator setpoint of 1.03, because it is equivalent to tripping at a discriminator setpoint that is [[ ]] and that is not a significant change considering the large CPR margin available to the SLMCPR. The slightly higher equivalent setpoint could cause the confirmation count to increase by one, but the scram delay due to this when oscillations are growing, is insignificant.

The impact on the amplitude is mitigated due to the use of a normalized signal in DSS-CD Period Based Detection Algorithm. In addition, multiple cells in the OPRM channel are typically approaching the amplitude discriminator simultaneously. A number of OPRM cells with no D and C level LPRMs, which are not affected by the bypass voiding attenuation, or with D and C level LPRMs with low bypass voiding, would provide the required OPRM amplitude performance.

The additional noise due to bypass voids also has negligible impact on the ability of the DSS-CD detection algorithm to detect instability oscillations because this noise is high frequency [[ ]] and is effectively filtered out by the double pole Butterworth "cut-off" filter (~1 Hz) in the OPRM equipment.

Thus the overall effect of bypass voids on the OPRM performance is insignificant.

Response to Part 1.4

TRACG does not assume zero bypass voiding. TRACG assumes that the worth of the void is independent of the distribution between the active channel, water rod and bypass, and that the cross-sections can be evaluated based on a volume averaged moderator density. This was formerly addressed in response to RAI 21-b in NEDE-32906P-A, Rev. 1, "TRACG Application for Anticipated Operational Occurrences Transient Analysis", April 2003.

The regular cross section generation process creates homogenized cross sections, node average reactivity, and pin powers at many depleted and instantaneous conditions. The effects of reduced moderation due to voiding are calculated by performing lattice physic statepoint analysis of different in-channel void conditions. During this process, the out-channel water and water rod are assumed to maintain the same density. Normally, this density is equal to solid water.

However, the cross sections are then parameterized as a function of node-average relative water density.

$$U = \left( \frac{A_f}{A_f + A_{byp} + A_{wr}} \right) \frac{\rho_f}{\rho_o} + \left( \frac{A_{byp} + A_{wr}}{A_f + A_{byp} + A_{wr}} \right) \frac{\rho_{byp}}{\rho_o}$$

where $\rho_f$ is the in-channel density with radial (bundle or channel) and axial dependence, $\rho_{byp}$ is the axially dependent bypass density, $\rho_o$ is a standard base density, and the subscripts of *f*, *byp* and *wr* indicate the in-channel, bypass, and water rod regions of the lattice.

PANACEA uses a core average axially zone model for the bypass region. TRACG has the ability to model the bypass regions as explicitly defined axial and radial zones. Additionally, TRACG has the ability to model the inside water rod moderator region for purposes of evaluating void fraction. By evaluating the density (or voiding) of the moderator in the bypass, the water rod, and the in-channel regions of a specific node, TRACG and PANACEA determine the nodal average moderator density.

$$U_{ijk} = \left( \frac{A_f}{A_f + A_{byp} + A_{wr}} \right) \frac{\rho_{ijk}}{\rho_o} + \left( \frac{A_{byp}}{A_f + A_{byp} + A_{wr}} \right) \frac{\rho_{byp,k}}{\rho_o} + \left( \frac{A_{wr}}{A_f + A_{byp} + A_{wr}} \right) \frac{\rho_{wr,k}}{\rho_o}$$

where $\rho_{f,ijk}$ is the in-channel density with radial (bundle or channel) and axial dependence, $\rho_{byp,k}$ is the axially dependent bypass density, and $\rho_{wr,k}$ is the axially dependent water rod density for each bundle modeled.

The combination of these assumptions is that the nuclear parameters are insensitive to the spatial location of a void. The effects of bypass and/or water rod voiding are captured in this manner. While there is some sensitivity to the location of the void, this sensitivity is below the level of uncertainty in the methodology.

The lattice data generated by TGBLA is generated at three void points and assumes no bypass or water rod voiding. The three void points are defined as 0%, 40%, and 70% in-channel void fractions respectively. The TGBLA generated neutronic data is created as a function of exposure from 0.0 GWd/st (BOL) to 65.0 GWd/st or higher for each void point and the lattice overall moderator density is provided as a base parameter for subsequent parametric fitting.

From the data provided in the response to RAI 1.1, the void fractions during the 2RPT transient in the upper regions of bypass could reach [[
]]. Under these conditions, the neutronic parameters in nodes that experience bypass and water rod voiding would be modeled as nodes of equivalent overall moderator density but where the bypass and water rod regions were evaluated as solid or zero void water by the lattice physics model.

To demonstrate the uncertainty in nodal reactivity and average pin fission density for this inter-nodal spatial moderator density difference, evaluations using MCNP and TGBLA were performed. Evaluations at 0, 40, and 70% in-channel void fractions represent the "production" void state conditions. Additional cases were evaluated at a 85% in-channel void fraction with

25% water rod and 10% bypass voiding, as well as 90% in-channel void fraction without water rod or bypass voiding. The latter two conditions are used to evaluate the uncertainty for the evaluation of the fitted "production" data at high in-channel and bypass void conditions. An additional case at 55% in-channel void fraction was generated to demonstrate the fitting uncertainties for interpolated void conditions. For exposed conditions, the depletion conditions for determining isotopic content of the lattice of interest are based upon a 70% in-channel state. The evaluations to determine the fitting uncertainty are generated by changing the moderator density to reflect the lattice state of interest.

The lattice reactivity from TGBLA06 represented by the infinite k-infinity at 0, 40, and 70% in-channel void fraction is fitted as a function of overall lattice moderator density and then used to evaluate the lattice reactivity for moderator density conditions expected in the MELLLA+ 2RPT event. [[

]]

Figure 1-14 demonstrates the agreement between the "fitted" data and the explicitly calculated data for reactivity for a typical lattice at several depletion points. The acceptable uncertainty bands (two-sigma) are attached to the 200 MWd/st data points to demonstrate that the fitted data falls with two-sigma of the fitted line. The deviations observed in Figure 1-14 between the extrapolated and interpolated k-infinity results are significantly below two-sigma uncertainty value.

For CPR, the effects of pin fission density (or rod power) on the R-factor generation are also of interest. The current uncertainty for fission density is a [[ ]]as documented in the Methodology and Uncertainties for Safety Limit MCPR Evaluations, (NEDC-32601P-A). The value is derived from an averaging of the TGBLA versus MCNP results for numerous lattices that represent the BWR design fleet. To demonstrate the uncertainty for out-channel and water rod voiding, the "production" void state data for a vanished (upper) zone lattice at 0, 40, and 70% void fractions has been quadratically fitted. A comparison of how well these fits predict pin fission densities versus average moderator density is of interest.

Both MCNP and TGBLA were used to evaluate the pin fission densities for the explicit void states of interest. The computed fission densities are then compared to the fit generated fission densities and the RMS (root mean square) of the differences is generated. Tables 1 and 2 show the uncertainties for interpolated and extrapolated data for the three lattice state conditions.

From the TGBLA based analysis in Table 1-1, an uncertainty of [[ ]] is calculated for the 90% in-channel void without bypass and water rod voids and [[ ]] is calculated for the 85% in-channel void with 10% bypass and 25% water rod voiding. For the interpolated point of 55% in-channel voids, the uncertainty was observed to be [[ ]] for TGBLA. From the MCNP based analysis in Table 1-1, an uncertainty of [[ ]] for the 90% in-channel void

without bypass and water rod voids and [[ ]] for the 85% in-channel void with 10% bypass and 25% water rod voiding. The uncertainty for the interpolated point at 55% in-channel voids, the uncertainty was observed to be [[ ]]. The larger value of the MCNP results is expected since the statistical uncertainty of approximately [[ ]] is convoluted within the comparison.

Table 1-2 is a repeat of the previous analysis using a different lattice design to demonstrate the consistence of the fitting approximations.

Both reviews of the fitting uncertainty for voiding greater than 70% in-channel along with voiding in the bypass and water rod demonstrate that the [[

]].

The final conclusive assessment of whether these additional uncertainties affect the ability of TRACG to be used for DSS-CD is demonstrated by data. The LaSalle 2 instability event of March 1988 has been evaluated in the TRACG Qualification report (NEDE-32177P). The oscillation periods and amplitudes, including the APRM scram prediction, agree well with the data and timing of the actual event. Examination of the TRACG simulation of this event (using a detailed bypass axial nodalization) shows over [[ ]] the active fuel region and over [[ ]] in the water rods prior to the onset of significant oscillations. More significantly, bypass and water rod voiding increases to much higher levels of voiding during the oscillations. Yet, since the aforementioned uncertainties would be present in this simulation, it may be concluded that the presence of bypass and water rod voiding do not affect the ability of TRACG to capture oscillation frequency as required by the DSS-CD algorithm.

Additional disposition of concerns on CPR are addressed in the response to RAI #19.

**Table 1-1: Fitted Fission Density Uncertainty Analysis for 10x10 lattice A at 0.0 MWd/st Exposure**

| Lattice Void Condition | Average Moderator Density | TGBLA Uncertainty | MCNP Uncertainty |
|---|---|---|---|
| [[ | | | |
| | | | {3}]] |

**Table 1-2: Fitted Fission Density Uncertainty Analysis for 10x10 lattice B at 200.0 MWd/st Exposure**

| Lattice Void Condition | Average Moderator Density | TGBLA Uncertainty | MCNP Uncertainty |
|---|---|---|---|
| [[ | | | |
| | | | {3}]] |

Figure 1-1, Schematic of Bypass and Upper Plenum Regions

[[

]]

Figure 1-2, Circulation in the Top of the Bypass

[[

]]

Figure 1-3, Subdivision of Top Level of Bypass

[[

]]

Figure 1-4, BWR/6 Circulation Flow

[[

]]

Figure 1-5, BWR/6 Bypass Void Fraction

[[

]]

Figure 1-6, BWR/6 Radial Liquid Velocity at the Top of the Bypass (Level 7)

[[

]]

Figure 1-7, BWR/6 Liquid Velocity at the Top of the Bypass

[[

]]

Figure 1-8, BWR/6 Vapor Velocity at the Top of the Bypass

[[

]]

Figure 1-9, BWR/6 Void Fraction at the Top of the Bypass in the Central Ring
(Refined Bypass Nodalization)

[[

]]

Figure 1-10, Void Fraction at the Top of the Bypass in the Peripheral Ring
(Refined Bypass Nodalization)

[[

]]

Figure 1-11, BWR/6 Core Average Power Void Fraction

[[

]]

Figure 1-12, BWR/6 Core Power

[[

]]

Figure 1-13, BWR/6 Circulation Flow

[[

]]

Figure 1-14, Fit Uncertainty to TGBLA06 Reactivity

[[

]]

**NRC RAI 2.**

See Fig. 3.7-12 NEDE-32176P, Rev. 2. Why doesn't noding study converge? Will increasing the number of nodes always change the results and if so, will the change always be conservative (i.e. predict larger and larger decay ratios)?

**GE Response**

Figure 3.7-12 from the TRACG Qualification Report (NEDE-32177P) shows that there is a sensitivity of the decay ratio to the node size. Figure 3.7-12 shows results for [[ ]] nodes for the test section. In the cases with [[ ]] nodes, the nodes for the [[ ]] nodes respectively. In the cases with [[ ]] respectively. The results of the sensitivity studies show that the decay ratio increases as the node size is decreased and decreasing the node size for the bottom nodes where the axial void fraction gradient is steepest captures that most of the effect. Based on these results it is estimated that the decay ratio would increase by [[ ]] for the fully converged case with an infinite number of nodes relative to the [[ ]] case for a decay ratio close to 1.0. An additional sensitivity study with [[ ]] nodes is fully in line with this estimate (see Figure 2-1 below for the 3.997 MW case).

Based on these results one could assume that the decay ratio would be underpredicted due to the numerical damping. However, comparisons to experimental data as shown in Figures 3.7-14 through 3.7-19 show that the decay ratio is overpredicted. A major reason for this overprediction is the one-dimensional hydraulic model used in TRACG and similar codes. In a fuel channel, the fluid velocity will vary across the cross section of the channel. The fluid velocity will be highest in the center of the channel and the fluid velocity will be low in the peripheral region next to the channel wall. Therefore, a density perturbation will travel with different velocities in different regions of the channel, and as a result the perturbation will be smeared and damped as it travels up the channel. This is a real physical damping, which is neglected in the one-dimensional model. The results of the qualification against data and the sensitivity studies show that the neglected physical damping is larger than the numerical damping introduced by the numerical scheme, and that density waves and thermal hydraulic instability are conservatively predicted by the one-dimensional TRACG model.

Figure 2-1. Figure 3.7-12 including a 160-node case.

[[

]]

**NRC RAI 3**

Why is changes to numerical methods allowed without NRC approval, when improved convergence has been shown to produce inaccurate results (i.e. implicit method converges better, but explicit method is more accurate for instability calculations)?

**GE Response**

This statement is a carry-over from a similar statement in the TRACG AOO LTR (NEDE-32906P-A). Due to the demonstrated sensitivity of density wave oscillations to the numerical scheme, this statement should be changed to: "changes to the numerical method that have insignificant impact on or would lead to an increase in decay ratio or oscillation amplitude can be introduced without NRC approval. Changes to the numerical method that lead to a reduction in decay ratio or oscillation amplitude should not be introduced without NRC approval."

**NRC RAI 4**

Is the numerical method selected on a component by component basis? If so how are the inconsistencies between numerical methods handled to ensure conservation of mass and energy at boundaries between explicit and implicit components?

**GE Response**

The numerical method is selected on a component-by-component basis. For applications to stability the explicit integration is used for the channel component, other components use the implicit numerical method. When a component using an implicit numerical method is connected to a component using the explicit numerical method, the new time step fluid properties are convected between the two components. Thus the component using the implicit numerical method is fully implicit for all nodes. The explicit component is fully explicit for all nodes except for a node connecting to an implicit component, which will use a mixture of old time step and new time step properties in the convective terms. Old time step properties are used in the convection to other cells in the explicit component and new time properties are used in the convection at a face connecting to an implicit component. See also Figure 4-1, that shows the choice of old time step property "$\varphi^n$" or new time step property "$\varphi^{n+1}$" for the convective terms for a combination of two components using different numerical methods. With this approach mass and energy balances are conserved.

Additional information on the sensitivity to the mixed mode integration is contained in the response to RAI 15.

**Figure 4-1. Convective Terms at a Junction Between Components Using Different Numerical Methods.**

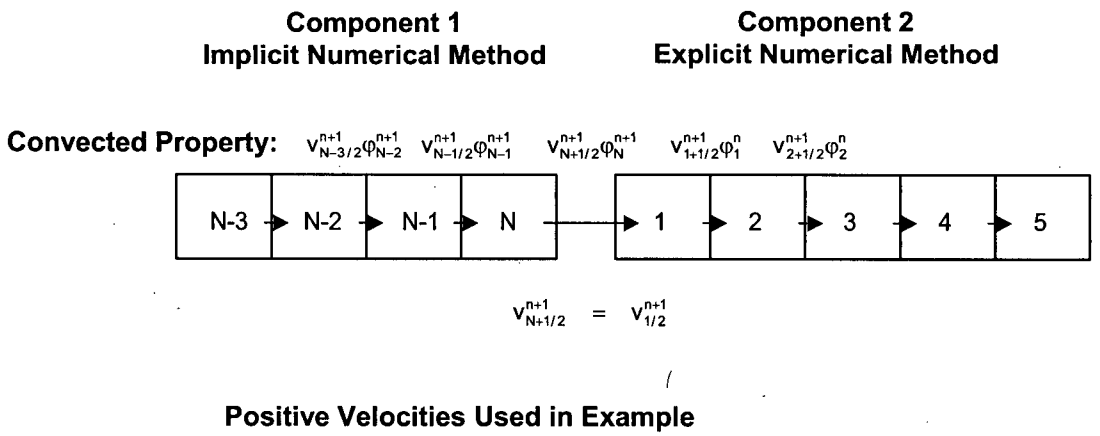

**NRC RAI 5**

Effect of time level differencing for the change in momentum flux (i.e. VdelV) on transient results (see Eq. 3.2-8 in NEDE-32176P, Rev. 2)? The time level for the VdelV term is not consistent and will introduce error into the calculation. Is the error significant and will it grow with time?

**GE Response**

There are several reasons why thermal hydraulic instability is not sensitive to the form of the convective term in the momentum equation (VdelV). First, the particular form of this term using a mixture of old and new time step properties as documented in the TRACG Model Description (NEDE-32176P) Section 8.2.1.1 is used in order to allow large time step sizes exceeding the Courant Limit for slow transients where dynamic effects are insignificant. In TRACG the automatic time step size control will reduce the time step size for fast transients where dynamic effects may be important, and since the error is of second order, the impact of this error will vanish for small time step sizes. This has been evaluated by sensitivity studies on the maximum allowed time step size for e.g., the PSTF blow down tests as documented in the TRACG Qualification report (NEDE-32177P Section 3.1.5.4. These sensitivity studies showed insignificant sensitivity to the maximum allowed time step size. Secondly, thermal hydraulic instability is controlled by density wave perturbations and is not sensitive to dynamic effects.

However, in order to close out the issue, a sensitivity study has been performed where the convective term in the momentum equation was changed to use only old-time step properties, i.e., to a purely explicit form. The result of this sensitivity study is shown in Figure 5-1. It is seen that the impact of the form of the convective term in the momentum equation on decay ratio (or growth rate) is small, approximately [[ ]]. This sensitivity is insignificant compared to the [[ ]] margin applied in stability calculations.

**Figure 5-1. Sensitivity to Form of the Convective Term in the Momentum Equation.**

[[

]]

**NRC RAI 6**

6.1 Figure 5 shown the scram time of DSS-CD. Please provide the scram time without using DSS-CD (i.e, using the existing detection and suppression method);

6.2 Please provide the basis of using 30% uncertainties and explain why it can bound the TGBLA/PANACEA uncertainties.

6.3 Please provide the revised TRAC-G code or TRACG graphics dump/input file using the correct void feedback formula.

**GE Response**

Response to RAI 6-1

The trip times using DSS-CD and Option III solution are provided in Table 6-1.

Response to RAI 6-2

The transient nuclear responses as related to the biases and uncertainties in the nuclear methods are dominated by the [[

]] Based on this observation, it was proposed that a variation of [[ ]] in the void coefficient would reasonably bound any errors that the NRC staff could imagine as being attributable to the lattice physics models and/or the 3D kinetics model. This value was proposed since it is known from experience that the calculated transient power responses when compared to the available transient plant data will reproduce the plant data using a void coefficient uncertainty within the range of [[ ]]. The fact that the proposed [[ ]] variation is bounding has subsequently been separately validated as described in the following paragraph.

The normalized %bias and %standard deviations in void coefficient based on TGBLA04-to-MNCP01 comparisons were shown in Figure 5-1 of NEDE-32906P-A, Revision 1 for different exposures and in-channel void fractions. Rather than directly apply the values from the figure, it is more convenient to use digital values on which they are based. This has been done both for the TGBLA04 dataset used to support applications of TRACG02 and the TGBLA06 dataset used to support applications of TRACG04. For the TGBLA04 dataset the mean void coefficient error averaged over all exposures and all void fractions is [[ ]]. For the TGBLA06 dataset the mean void coefficient error averaged over all exposures and all void fractions is [[ ]]. Note that these ranges are consistent with the general observation that TRACG can reproduce the available transient BWR power data by considering a variation of the void coefficient in the [[ ]] range. Based on the cited TGBLA04 and TGBLA06 datasets compared to MCNP, the assumed bounding range of [[ ]] represents a level of significance of [[ ]] sigma for the TGBLA04 dataset and [[ ]] for the

TGBLA06. The NRC stated position is that in the absence of rigorous quantification of the uncertainty band, a ±2 sigma variation is deemed reasonable.

GNF contends that the maximum plausible span in the void coefficient is easily bounded within the assumed [[ ]] range and that the increased level of conservatism beyond the approximate [[ ]] range that analyses supports will certainly bound any sources of error that the NRC staff can reasonably postulate.

Sensitivity studies have been performed applying the ±30% uncertainty in the void reactivity coefficient to the fast event with the highest growth rate and to the intermediate event with the slowest growth rate. The margin to the SLMCPR is provided in Table6-2.

Response to RAI 6-3

The CD provided in Enclosure 3 contains the graphics dump and input file for the BWR6 100100-120F case.

**Table 6-1**
**Trip Times**

| Case | Trip Time for DSS-CD (Seconds) | Trip Time for Option III Solution (Seconds) |
|---|---|---|
| Nominal | [[ | |
| Minus 30% | | |
| Plus 30% | | ]] |

**Table 6-2**
**MCPR Margin to the SLMCPR**

| Case | Fast Event 100100-120F 2RPT Normalized/Bounding | Slow Event 10080 to 45% Rated Core Flow Normalized/Bounding |
|---|---|---|
| Nominal | [[ | |
| Minus 30% | | |
| Plus 30% | | ]] |

**NRC RAI 7**

Similar to RAI #1, the TRACG case provided by GENE ( PHE_10080_2PT_2TR_RENT_ PLOT.INP ) calculated the water rod internal voiding at the end of 100 seconds 2RPT transient. The exit void fraction of CHAN24 water rods is about 41%. Please address the following questions regarding the water rods internal voiding and its impact on the TRACG DSS-CD application methodology.

7.1 Does the current cross-section generation methodology have the capability to analyze voiding in the water rods? If it does, please explain how the void is being treated. If not, please explain what the impact of this model deficiency to the DSS-CD application.

7.2 Does the PANANCEA 3-D core steady state simulator have the capability to analyze voiding in the water rods? If it does, please explain how the void is being treated. If not, please explain what the impact of this model deficiency to the DSS-CD application.

7.3 It is not clear how TRACG handles the water-rods voiding. Therefore, with water rods voiding, is the current GE reload methodology still valid for GE-10 to GE-14 fuel applications? Please provide detailed discussion regarding how the water rods void fraction is being modeled and examine the adequacy of the method to model the 2RPT transient. Please explain how the uncertainty of SLMCPR and CPR are evaluated when none-zero water rods void exists.

**GE Response**

Response to Part 7.1

Please see the response to RAI 1.4.

Response to Part 7.2

PANACEA uses a single core average bypass region. Water rod flows are lumped with the out-channel flows, but the [[

]]

Once the total water rod and bypass flow is determined, PANACEA does perform a momentum and heat balance on the bypass region. The heating components for the bypass include direct moderator heating, control blade heating, conduction from heating in the channel, conduction from the active to bypass region through the channel, and other gamma heating components. If bypass flow rate is low enough or heat deposition high enough, the PANACEA model will calculate voiding in the bypass region.

The PANACEA model does not directly affect the DSS-CD application as it is only used to prepare a restart file (containing cross sections, exposure basis, etc.) for TRACG. When used to quantify thermal margin for DSS-CD, TRACG will converge the initial steady-state using the TRACG water rod and bypass model geometry prior to the time-dependent stability analysis.

For the neutronic impact of water rod voiding, please see the response for RAI 1.4. For the impact of water rod voiding on the R-factor, please see the response for RAI 1.4 and RAI 18.

Response to Part 7.3

TRACG solves the mass, momentum and energy equations for the water rod when this model is applied. The water rod flow is calculated based on the pressure drop characteristics of the water rod, which include the static head in the water rod and the frictional characteristics of the inlet and exit flow. Energy transfer to the fluid in the water rod includes conductive heat transfer through the water rod wall and direct moderator heating. The void fraction in the water rod is then calculated from the mass and energy balances coupled with the momentum equations. The hydraulic models used for the water rods are the same as used for the in-channel and bypass flow. In providing feed back to the kinetics solution a volume averaged fluid density is calculated for the in-channel flow, the water rod and the bypass region. The application range for these models and correlations cover a wide range of hydraulic conditions and geometries as documented in the TRACG Model Description (NEDE-32176P) including 8X8 to 10X10 fuel bundle designs. Critical power depends on the in-channel hydraulic conditions. The hydraulic conditions in the water rod have no impact of fuel rod heat transfer and dryout.

**NRC RAI 8**

TRACG qualification report cited FRIGG test data as the evidence to support the argument that TRACG has successfully modeled single channel density wave oscillation. Please provide the TRACG FRIGG assessment case input deck and relevant document about this test facility.

**GE Response**

A TRACG input deck for the FRIGG stability test facility is contained in the file FRIGG_P_307_P3997_T.INP. This case is for a pressure of 3.07 MPa, a power of 3997 kW and an inlet subcooling of 5 C. Normally a steady state calculation is first performed using the fully implicit integration scheme for all components and a large time step size. The components are extracted from the steady state calculation and the option for the integration scheme is reset to the explicit integration scheme. This new input deck is then used to perform the transient stability calculation. The supplied deck is the input for the transient calculation. The testing is documented in the document: "FRIGG Loop Project, Hydrodynamic and Heat Transfer Measurements on a Full-Scale Simulated 36-Rod BHWR Fuel Element With Non-Uniform Axial and Radial Heat Flux Distribution", FRIGG-4, Sweden 1970.

**NRC RAI 9**

Is there any set of normal or anticipated off-normal operating conditions for any reactor design that can have a power oscillation at a frequency outside the frequencies considered by DSS-CD? NEDC-33075P, Revision 3, Section 3-2, Page 3-2 indicates that cell signals are filtered to remove noise above 1 Hz and filtered again for frequencies below 1/6 Hz to obtain a time-averaged value. This implies that the signals of interest are between 1/6 Hz and 1 Hz. NEDC-33075P Revision 3, Section 3.4.1, Page 3-19 indicates that power oscillations occur within the frequency band of 0.3 to 0.7 Hz. T.H.J.J van der Hagen, A.J.C. Stekenburg, D.D.B. van Bragt, "Reactor experiments on type-I and type-II BWR stability," Nuclear Engineering and Design 200, 2000, pp. 177-185 indicate that for the Dodewaard natural-circulation BWR there is hydrostatic head instability that occurs at very low oscillation frequency (i.e. <0.1 Hz), at low pressure, low natural circulation flow and low coolant flow quality. Since this instability is controlled by the hydraulic parameters and is damped by neutronics feedback and since it occurs at such a low frequency, this type of instability would not be detected by DSS-CD. Is there differences in a typical BWR design relative to the Dodewaard reactor that preclude this type of instability for BWRs? If not does this type of instability occur at such a lower power level, that it does not represent a safety concern?

**GE Response**

The power oscillations of interest in an operating BWR are due to density wave transport through the core (also called Type 2 in the literature). The time period of oscillation is related to the transport time of voids through the core. The range of frequencies is typically between 0.3 to 0.6 Hz in the range of conditions between natural circulation and higher flows where oscillations could potentially occur. This range is easily bounded by the frequency range of 1/6 Hz to 1 Hz.

The low frequency oscillations noted at the Dodewaard plant are those denoted as Type 1 and are peculiar to natural circulation loops at low pressure. These are encountered when voids are first initiated in the riser (unheated region above the core), leading to an increase in natural circulation flow. The increase in flow quenches the voids, leading to a reduction in flow. The cycle is repeated, until an increase in the power level establishes steady voids at the exit of the flow loop. The time period of these oscillations was of the order of 10 s for Dodewaard, corresponding to enthalpy transport through the core and riser. In Dodewaard, these flow oscillations occurred while there was single phase flow in the core. The voids are initiated at the top of the riser because of the lower saturation temperature (significant at low pressures). Thus there is negligible reactivity feedback and huge margins are maintained to thermal limits.

Such oscillations are not possible in forced circulation plants that start up with pumped flow. A Type 1 instability region does not exist for forced circulation.

**NRC RAI 10**

NEDC-33075P, Revision 3, Section 4.4.3.3, page 4-14 indicates that CSAU bounding relative uncertainty for the oscillation relative DCPR is 250%. How is this uncertainty calculated? An uncertainty of 250% implies, either an important phenomena is not modeled or not modeled correctly, or there is some error in the code or the uncertainty calculation is not consistent or the model is very sensitive to small changes in the input/parameters. The nominal and bounding Final MCPR values in Tables 4-4 and 4-5 do not seem to support this large uncertainty. For example for case 10080RG6, the nominal and bounding Final MCPR values are 1.39 and 1.33 which implies a relative percent difference of 4.3%, which is significantly different than 250%. The nominal and bounding margin to SLMCPR for this same case are, 0.27 and 0.21 which implies a relative percent difference of 22.2%, which is still a factor of 10 smaller than 250%. The uncertainty of 250% appears to be based on comparing CPR results in Figs. 4-5 and 4-19 in NEDC-33075P, Revision 3 at specific times during the transient. However, the bounding CSAU results and the nominal results are for two different transient responses. The changes in boundary conditions and modeling parameters in TRACG make it inappropriate to compare CPR at specific times.

**GE Response**

DSS-CD LTR Section 4 discusses a number of different uncertainty elements that should not be confused.

First and foremost, the DSS-CD detection algorithm setpoints are established independent of the TRACG confirmatory calculations to ensure the earliest oscillation suppression with appropriate considerations of spurious scram avoidance. Specifically, reactor scram occurs with only a limited number of oscillation periods permitted and just above the noise level. The final MCPR for anticipated events is expected to remain well above the SLMCPR, independent of the TRACG analysis. This approach is different in principal from the original Option III approach, which establishes the amplitude setpoint such that the final MCPR is approximately just above the SLMCPR. This difference is critical to the understanding of the basis for the TRACG MCPR confirmation analysis.

The DSS-CD original (and current) approach is to avoid detailed TRACG uncertainty calculations for solution applications. To that end, the DSS-CD design provides ample margins to all solution aspects, including MCPR margin. It is expected, that [[

]] This however requires significant effort and is not needed for DSS-CD because of its inherent margin. Instead, a conservative and practical approach is taken for DSS-CD that avoids unnecessary academic minutiae.

The DSS-CD LTR uncertainty evaluation includes two separate analyses in Section 4. [[

]] and provides a successful demonstration that TRACG is behaving according to expectations during an instability event with adequate responses to changes in the key parameters. This analysis is performed for demonstration only and is not used in the application procedure. The second analysis consists of the DSS-CD application procedure and consists of two elements. [[

] which is judged to be very conservative. T his uncertainty is somewhat arbitrary but very high. It is expected that [[

]] Since the DSS-CD design provides significant margin flexibility, a detailed CSAU analysis is avoided, and a very conservative value is used instead.

**NRC RAI 11**

The approach taken for including uncertainty into the TRACG power oscillation calculations was to use an uncertainty of 20% for the reduced flow DCPR/CPR and a 50% uncertainty for the oscillation DCPR/CPR. Should an additional uncertainty associated with noding be included in these calculations? NEDE-33147P, Draft B, Section 4.2.2, Page 4-3 indicates that X3 noding has an uncertainty of ~10% in the calculated decay ratio. If the nominal and bounding cases were run with the same noding, then the bounding uncertainties given above do not reflect uncertainty associated with noding.

**GE Response**

The X3 noding scheme has not been explicitly treated in the DSS-CD LTR. This impact is expected to be small since the X3 noding scheme resulted an uncertainty of about 10% in the calculated decay ratio. This indicates that the growth rate could be under-predicted by about 10%. However, for the DSS-CD solution, a higher growth rate tends to be beneficial to the DSS-CD Confirmation Density Algorithm (CDA) since the plant will tend to scram earlier. This has been confirmed with TRACG sensitivity runs with a higher decay ratio (which translates into a higher growth rate). These TRACG runs with a high growth rate of about 1.10 to 1.15 show that the DSS-CD CDA will scram slightly earlier. An increase in power response results in a decrease in the time to reach the amplitude setpoint.

**NRC RAI 12**

Virtual mass term is stated to be important for bubbly flow. Comparisons to steady-state void profile data, do not test the transient nature of the virtual mass term. There is some uncertainty associated with the coefficients in the virtual mass terms and the form of the virtual mass terms. Varying of coefficients in the virtual mass terms and of the form of the virtual mass terms does not appear to be part of the bounding analysis used to determine the bounding uncertainty for the change in CPR due to flow reduction and due to oscillations. Have there been any power oscillation calculations performed with changes in the virtual mass model in TRACG?

**GE Response**

TRACG has been qualified against steady state as well as transient void fraction data and documented in the TRACG Qualification Report (NEDE-32177P) Sections 3.1 and 3.4.3. These tests can be categorized into three groups dependent on the transient characteristics of the tests as shown in Table 12-1.

In order to address the last part of the question relating to the impact of the virtual mass term on thermal hydraulic stability a sensitivity study to evaluate the impact of the virtual mass term has been performed. Figure 12-1 shows the results of two calculations with and without the virtual mass term. It is seen that the impact of the virtual mass term on decay ratio (or growth rate) is small, approximately [[ ]]. This sensitivity is insignificant compared to the [[ ]] margin applied in stability calculations.

There is a slight increase in the time period for the oscillation when the virtual mass is eliminated. When the virtual mass is absent the vapor accelerates faster to reach the equilibrium velocity, where there is a balance between interfacial shear and buoyancy. This effect is mainly important downstream of the transition from churn flow to dispersed annular flow, where there is a large increase in the relative velocity over a short distance. Thus, there is an increase in the vapor velocity and a corresponding decrease in the liquid velocity in a short region downstream of the transition to dispersed annular flow in the absence of the virtual mass term. Since density waves travel with the velocity of the dispersed phase, the decrease in the liquid velocity in this region leads to an increase in the transit time for the density waves and a corresponding increase in the time period for the oscillation. The effect however is small. When the virtual mass term is removed, the frequency changes from [[ ]] Hz.

Non-proprietary Version

**Table 12-1 Void Fraction Qualification Data Base**

| Adiabatic Void Fraction Tests | Heated Void Fraction Tests | Transient Tests |
|---|---|---|
| No temporal acceleration<br>No spatial acceleration | No temporal acceleration<br>Spatial Acceleration | Temporal Acceleration<br>Spatial Acceleration |
| [[ | | ]] |

Figure 12-1. Sensitivity to Virtual Mass Term.

[[

]]

**NRC RAI 13**

Please provide a figure of the channel grouping with the ring 1, 2, and 3 boundaries included. For example, Fig. 5-7 of NEDC-33075P, Revision 3 with the ring 1, 2, 3 boundaries included. NEDE-33147P, Draft B, Section 4.2.6, Page 4-5, implies that channel groups may include channels/bundles from both Ring 1 and Ring 2 of the TRACG vessel noding. The channel to vessel connections are apparently adjusted to ensure that the ratio of the number of bundles in Ring 1 to Ring 2 is roughly the ratio of the flow areas of Ring 1 to Ring 2. If this is to address channels/bundles that are on the boundary between the Rings 1 and Rings 2, then a more appropriate modeling method would be to assign the boundary bundles to either Rings 1 or 2, depending upon whether more of the channel is in Ring 1 or 2. The lower plenum, volumes and flow areas would be adjusted for Rings 1 and 2 consistent with the total number of channels/bundles that are actually simulated in rings 1 and 2. The channel grouping in Fig. 5-7 of NEDC-33075P, Revision 3 for channel group numbers 20 and 30, extents from the center of the core to the periphery of the core. Which of the 3 rings is channel groups 20 and 30 included into in the TRACG vessel model? If TRACG allows for multi inlet connections for a single CHAN component, then inlet connections for channel groups 20 and 30 can be spread across all three rings. If the fluid conditions in the lower and upper plenum are uniform in the radial direction, then this type of modeling approximation may not be important.

**GE Response**

Figure 13-1 shows the ring boundaries imposed on the channel grouping for BWR6 Instability Event. In this model, which is typical for stability modeling, only two rings are used; an inner ring and one for the peripheral channels. In this case, all but the peripheral channels are assigned to Ring 1. [[

]]

**Figure 13-1. Channel Rings used in the BWR/6 Instability Model**

[[

]]

**NRC RAI 14**

NEDC-33075P, Revision 3, Section 4-5, page 4-16, refers to Table 4-7. There is no Table 4-7. I think the text should refer to Table 4-6.

**GE Response**

GE agrees the correct reference is Table 4-6. Revision 4 of NEDC-33075P, issued in July 2004, identifies the correct reference.

Non-proprietary Version

**NRC RAI 15**

What is the magnitude of the error associated with mixed time level integration of implicit 3D vessel cells connected to explicit fuel channel components? What is the effect of this error on MCPR calculations for a TRACG power oscillation? The coupling of an explicit fuel channel component with an implicit vessel component results in the shared cell edge or junction to be solved explicitly. Specifically, mass and energy that is fluxed across the junction or boundary between the explicit and implicit component is at old time (i.e. explicit). However, that implies the coupling cell in the lower and upper plenums (i.e. the vessel cells connected to the fuel channel component inlet and outlet) have cell edges with different time levels for the fluxing mass and energies (see Fi.g below). For example, the upper plenum cell connected to the top of the fuel channel component has old time mass and energies fluxing across the bottom of the 3D cell and new time mass and energies fluxing across the top and sides of the 3D cell. What is the numerical error associated with this approximation? Time integration schemes are typically, explicit (i.e. fluxing mass and energies are old time), implicit (i.e. fluxing mass and energies are new), or somewhere in between (i.e. Crank-Nicolson type with half old and half new time). However, time integration schemes are normally applied uniformily at all cell edges for a given cell. In the upper and lower plenums, the TRACG power oscillation calculations include a row of cells with explicit integration on one cell edge and implicit integration on the other cell edges. Would it be practical to run one typical power oscillation calculation with TRACG with all hydrodynamic components using the explicit integration scheme? A calculation of this type would provide an indication of the magnitude of the error associated with the mixing of the time level level integration schemes.

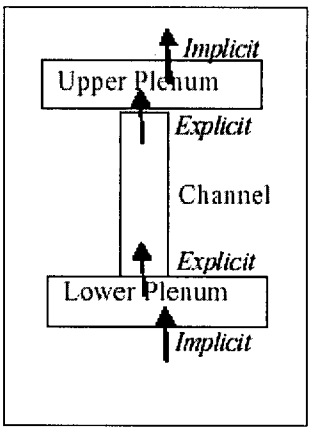


**GE Response**

The effect of the mixed time level integration has been evaluated by performing a sensitivity study for one of the FRIGG stability cases. The explicit integration scheme is always used for the channel component. Two calculations were performed, a calculation where the implicit

integration is used and a calculation where the explicit integration scheme is used for the remaining part of the test loop outside the channel component. The results of these calculations are shown in Figure 15-1. [[

]].

**Figure 15-1. Sensitivity Loop Integration Scheme.**

[[

]]

**NRC RAI 16**

What is the magnitude of error associated with using extrapolated amplitude and shape functions for the thermal-hydraulic solution? NEDE-32176P, Rev. 2 Section 9.5, page 9.5-1 indicates that the amplitude function is extrapolated quadratically and the shape function is extrapolated linearly to estimate the power distribution for the thermal-hydraulic calculation. Because of the coupling between the thermal-hydraulic and 3D neutronics calculations it is advantageous to use some type of predictor method to estimate the new time power level and distribution to be used in the thermal-hydraulic calculation. The calculational sequence as described in Section 9.5 of NEDE-32176P, Rev. 2 is:

a) Estimate the power level and distribution at the end of this time step, based on quadratic extrapolation of the amplitude function and linear extrapolation of the shape function.
b) Advance the thermal-hydraulic solution one time step.
c) Update the point kinetics parameters.
d) Advance the amplitude function to the end of the thermal-hydraulic time step.
e) Obtain the delayed neutron precursor densities.
f) Recalculate the shape function if necessary. Recalculation of the shape function involves iteration with the amplitude function and reactivity step (i.e. Shape Step Iteration). The thermal-hydraulics, nodal cross sections and the delayed neutron precursor densities are omitted from the Shape Step Iteration. Shape function is recalculated every other amplitude/reactivity step.

The concern here is the thermal-hydraulic equations are advanced based on extrapolated amplitude and shape functions, but there does not appear to be an attempt to correct the thermal-hydraulic solution for the extrapolation error in power (difference is extrapolated power distribution versus actual power distribution calculated at the end of the time step). At the end of step f, the amplitude and shape function are consistent with each other, but are not consistent with the extrapolated amplitude and shape function used to solve the thermal-hydraulic equations. There are at least two approaches to get an indication of the error associated with this inconsistency:

a) Perform one typical TRACG power oscillation calculation with the thermal hydraulic, delayed neutron precursor densities, and nodal cross-sections included in the Shape Step Iteration. A calculation of this type would provide an estimate of the sensitivity of this error in the power calculation on the MCPR calculation. If this type of calculation is impractical, then option b) should be considered.

b) Include edits for this power error in a typical TRACG power oscillation calculation. For example, a time trace of the difference between the extrapolated amplitude function and the actual amplitude function would provide an indication of the magnitude of this error. A time integration of this error would provide the difference in total energy in the thermal-hydraulic calculation and total energy in the 3D neutronics calculation. The

error in the extrapolated shape function would require some spatial averaging to provide a useful number.

**GE Response**

[[

]]

**Table 16-1** [[

| | | | | |
|---|---|---|---|---|
| | | | | |
| | | | | |
| | | | | |
| | | | | |
| | | | | |
| | | | | |

]]

**NRC RAI 17**

In the "TRACG Model Description," NEDE-32176P, Rev. 2, Dec. 1999, in Section 6.6.6.2 on page 6.6-18, the following statement occurs:

"When a>0.9, the Bias critical heat flux is multiplied by 0.1(1-a)."

This represents a discontinuous adjustment factor. It does force the critical heat flux to zero as the void fraction goes to one. However, at a void fraction of 0.9, the adjustment factor is 0.01. Normally, these type of adjustment factors start at one go to zero, as the void fraction goes from 0.9 to 1.0. Is the statement wrong (i.e. should be 10(1-a)) or is the coding/model in error? For the BWR stability calculations CPR is predicted by the GEXL correlation, therefore the implementation of the Biasi correlation will have no effect, expect on non-fuel-rod heat structures (i.e. dryout for water rods, channel box walls, etc.). For a typical BWR stability calculation void fractions above 90% inside of a water rod or in the core bypass are not expected. However, if the statement is not consistent with the model as coded, then it does raise the concern that the documentation does not accurately representing the coding in TRACG.

**GE Response**

There is a typographical error on page 6.6-18. The multiplier to the Biasi correlation for $\alpha > 0.9$ should be:

$$10(1-\alpha) \text{ or } (1-\alpha)/0.1,$$

otherwise the correlation would be discontinuous. The coding is consistent with the above expression:

```
IF (ALP.GT.0.9) QPPBIA = QPPBIA*10.0*(1.0-ALP)
```

**NRC RAI 18**

The GEXL correlation is a function of the R factor, which is a parameter which characterizes the local peaking factor relative to the most limiting rod. For a given fuel rod bundle design, an R factor is determined and used in the evaluation of the GEXL correlation. However, the experimental data used to develop and verify the GEXL correlation for a given fuel rod bundle design is based on experimental test facilities that use electrically heated rods which include a set of local peaking factors based on expected normally power and void distributions. The actual local rod-to-rod peaking during a typically BWR instability transient could be significantly different than the local peaking factors used in the ATLAS loop and the Columbia University test loop. What is the impact or uncertainty associated with the TRACG CPR calculation given that the rod-to-rod peaking factors may be changing significantly with time during a typical BWR instability calculation? For example, consider a given fuel rod bundle design that includes one or more water rods for the purpose of flattening the rod-to-rod power peaking across the rod bundle. The R factor used for the evaluation of the GEXL correlation and the ATLAS tests used to develop and verify GEXL are based on the local peaking factors under normal operating conditions (i.e. no significant void fraction in the water rods and core bypass). However, during a BWR instability transient, the water rod and core bypass will experience significant void fractions. GE has already run MCNP calculations with voided water rod and core bypass so changes in the rod-to-rod peaking could be estimated from these calculations. Given the methodology for calculating the GEXL correlation R factor, then the effect of the changes in the rod-to-rod peaking on the R factor and upon calculated CPR could be estimated. The effect of changing peaking factors upon typical ATLAS test results, could be estimated by looking at changes in the relative magnitude in the A(i) GEXL coefficients that involve V(i) functions that depend upon the R factor for similar bundle designs with different rod-to-rod peaking. Another approach to address this issue would be to run tests with rod-to-rod peaking factors consistent with voided water rods and core bypass. Also, with significant voids in the water rods is it possible to have rod-to-rod peaking factors outside of the data base range for the GEXL correlation? The peak rod-to-rod peaking factors for the data base range for GEXL is indicated to be 1.61 for the corner rods and 1.47 for interior rods. Intuitively, voiding in the core bypass would tend to increase the interior rod peaking, while voiding in the water rod may tend to increase the corner rod.

**GE Response**

The R-factor is a parameter which accounts for the effects of the fuel rod power distributions and the fuel assembly local spacer and lattice critical power characteristics. Its formulation for a given fuel rod location depends on the power of that fuel rod, as well as the power of the surrounding fuel rods. A detailed description of the R-factor calculation method for GE14 can be found in NEDC-32851P, Rev. 1, Appendix A.

For fuel products prior to GE11, an axial zone length-weighted scheme was used to generate the bundle average R-factor. The method was based on an assumption that a uniform (flat) axial

void profile. The basis for "D" lattice bundles was an in-channel average void fraction of 60% and for other lattice types was 40% average in-channel void fraction.

For the GE11 and more recent fuel products, a scheme where [[
]] is used to generate the bundle average R-factor.

[[

]]. It was observed during the development of this R-factor weighting process that the bundle average R-factors were in-sensitive to the axial void shape and bundle average void fraction. It was also observed that the R-factor response to in-channel void fraction was a function of the lattice design.

To evaluate the response of the R-factor to the possible bundle void condition during a DSS-CD event, [[

]].

To evaluate the response of the R-factor to the use of extrapolated data above the standard 0, 40, and 70% calculated void points, [[

]].

To evaluate the response of the R-factor to the presence to bypass and water rod voiding, [[

]].

By comparing the original "production" basis R-factor to the [[

]].

Statistically combining this uncertainty with the overall GEXL10 uncertainty of [[ ]]. This increase in GEXL uncertainty is not significant to the modeling of the core during the DSS-CD stability event.

This observation leads to a conclusion that the original "production" R-factors are representative of the [[

]].

While there is considerable variability in the R-factor with increasing void fraction, the current methodology is representative of the characteristics of the operating domain.

Non-proprietary Version

**Table 18-1: Modified R-factor Uncertainty Analysis**

| Exposure (Gwd/st) | Production R-factor | [[ ]] | Delta | [[ ]] | Delta | [[ ]] | Delta |
|---|---|---|---|---|---|---|---|
| [[ | | | | | | | |
| | | | | | | | |
| | | | | | | | |
| | | | | | | | |
| | | | | | | | |
| | | | | | | | |
| | | | | | | | |
| | | | | | | | |
| | | | | | | | |
| | | | | | | | |
| | | | | | | | |
| | | | | | | | |
| | | | | | | | |
| | | | | | | | |
| | | | | | | | |
| | | | | | | | |
| | | | | | | | |
| | | | | | | | |
| | | | | | | | |
| | | | | | | | |
| | | | | | | | |
| | | | | | | | |
| | | | | | | | |
| | | | | | | | |
| | | | | | | | |
| | | | | | | | |
| | | | | | | | |
| | | | | | | | ]] |

**Figure 18-1, Bundle Axial Void Profile**

[[

]]

**Figure 18-2, R-factor Response for 70% Bundle Average Void Fraction**

[[

]]

**Figure 18-3, R-factor Response for 4-Void Point Model**

[[

]]

**Figure 18-4, R-factor Response for 20% Bypass/Water Rod Void Fraction**

[[

]]]

**NRC RAI 19**

In NEDE-32107P, Rev. 2, Section 9.5 on page 9.5-2, Eqs. 9.5-4, 9.5-5, and 9.5-6 are solved to obtain the delayed neutron precursor density at each 3D node in the 3D transient neutronics model. However, Eqs. 9.5-5 and 9.5-6 are dependent upon the new time solution for the amplitude function A(t) and Eq. 9.5-6 is dependent upon the new time solution for shape function, S(r, t). The time dependent solution for the shape function depends upon the amplitude function. Eq. 9.1-24 on page 9.1-8 includes the $B^2_{ti}$ term which is a function of the time dependent solution for the amplitude function. The amplitude function time dependent solution (i.e. Eq. 9.1-19) includes core averages for the shape function. Therefore, the equations sets 9.1-19, 9.1-24, and 9.5-2 are coupled. Section 9.5 explains how the shape function and amplitude function solutions are iterated in order to obtain a consistent solution for both the amplitude and shape functions. However, according to the text on page 9.5-3, the delayed neutron precursor density is not included in this iteration (i.e. shape step iteration). What is the impact of leaving the 3D node delayed neutron precursor density out of this iteration? Is it possible/practical to perform a TRACG calculation with the delayed neutron precursor density included in this iteration to determine the impact?

**GE Response**

The impact of leaving the 3D node delayed neutron precursor density completely out of the shape iteration would be that the fraction of delayed neutrons (approximately 0.005 to 0.0075) due to delayed neutron precursors would be distributed according to the converged flux shape from the previous time step rather than the current time shape. The approximation used in the solution is actually better than this for rather than assuming that nodal fluxes do not change with time, the solution approach assumes that the nodal flux amplitude changes with time but does so with the gradient given from the shape for the previous time step. This is the fundamental assumption associated with the separation of the flux into its spatial and temporal components per Eq. 9.1-15. Please note how the gradient term FTRM is considered in Eqs. 9.5-5 and 9.5-6 and how these integrals fold into Eq. 9.5-4. Certainly it is possible to modify TRACG02 to include the precursor density shape update in a different way; however, such a modification is not warranted in view of the fundamental assumption of Eq. 9.1-15 and our assessments to quantify the sensitivity of the solution to the solution scheme as described in the following paragraph.

Time step size sensitivities for the 3D neutronics solution for AOO transients are documented in Section 6.9 of NEDE-32177P, Rev. 2. The results show that the time step size used to advance the flux shape step in time is being adequately controlled to maintain accuracy. Additional sensitivity studies were performed in response to RAI #6 in NEDE-32906P-A, Rev. 1 to quantify the impact of varying other parameters related to the neutron kinetics solver. These included sensitivities to the convergence criterion and the update frequency for the flux shape. These studies support the conclusion that convergence of the 3D power shape is sufficiently tight so that there is a negligible impact on the critical safety parameters. The key parameter for AOO

analyses is ΔCPR, one of the same critical parameter as for stability analyses. However, for channel power oscillations in the frequency range associated with an instability event, the magnitude of the ΔCPR response is not sensitive to the amplitude of the power oscillation because the fuel thermal time constant is much larger than the oscillation period. For purposes of the DSS-CD algorithm, the critical parameter is the frequency of the oscillation. The qualification calculations documented in Sections 7.4 and 7.5 of NEDE-32177P, Rev. 2 show that the maximum difference of [[ ]] Hz between the TRACG calculated and measured frequency occurs for regional oscillations. (See the response to Questions 21 for further discussion.) We have conservatively assumed a 1-sigma uncertainty of [[ ]] Hz when performing our uncertainty analyses. The DSS-CD algorithm is designed to detect oscillations with periods in the range of [[ ]] seconds ([[ ]] Hz). The Leibstadt tests indicate a period of [[

]] More margin is allowed for the lower frequencies because for lower frequencies (longer periods) the magnitude of the flow change is larger and this is the dominant influence in determining the change in CPR. For modern higher-energy cores, the power oscillations tend to begin at higher flow rates so that the tendency is for the frequency to increase and the period to decrease. Note that this is in the direction that leads to a less severe CPR response.

**NRC RAI 20**

The amplitude function equation given by Eq. 9.1-19 on page 9.1-6 of the report NEDE-32176P, Rev. 2 includes the delayed neutron precursor densities in the $G_n$ term which is a weighted core average of the delayed neutron precursor densities? Solution of Eq. 9.1-19 results in a $G_n(t)$ for n = 1, N. However, Eq. 9.5-4 is solved to determine the delayed neutron precursor densities for each 3D node in the model (i.e. $C_n(r, t)$). Based on the definition for $G_n$, the $C_n(r, t)$ solutions imply another solution for $G_n(t)$. Is there any attempt to reconcile these two solution methods for $G_n(t)$? During a typical BWR instability transient is there significant difference between $G_n(t)$ from Eq. 9.1-19 and implied from the solution of Eq. 9.5-4? Would it be practical for a typical BWR instability transient to calculate $G_n(t)$ using both methods and determine the difference?

**GE Response**

The expression for $G_n(t)$ on page 9.1-6 is the definition of the weighted core average of the delayed neutron precursor densities ($C_n(r,t)$). The other solution that the question implies appears to be that obtained by integrating the expression for $dG_n / dt$. This integration is not performed because it is never needed. The intent of the equations on page 9.1-6 was to show the elements that go into the determination of the core-wide amplitude function. [[

]] Any comparison with the summation $G_n(t_{i+1})$ does not indicate the fidelity of the temporal solution for $C_n(r,t)$, it only indicates the appropriateness of the weighting function used to collapse the nodal values to the core-averaged value $G_n(t)$. The choice of such a weighting will influence the temporal derivative of the amplitude function. For one-group formulations, it is typical (as we have done) to choose the weighting function to be the adjoint flux.

The adequacy of the approach is assessed by the comparison with experimental data. For regional instabilities, the magnitude of the channel oscillations have been compared for the Leibstadt stability tests in Section 7.5 of NEDE-32177P, Rev. 2. The agreement between the calculated LPRM peak-minimum divided by the average in Table 7.5-2 is well within the range of what one would expect [[

]]. (See the response to RAI #21.) [[

]] Table 7.5-2 of NEDE-32177P, Rev. 2 shows the comparisons between the calculated and measured frequencies. These comparisons are well within the range of uncertainty that the DSS-CD algorithm has been designed to address. See the response to Questions 21 for further discussion.

**NRC RAI 21**

The single group transient diffusion model in TRACG is based on the assumptions that:

$$\frac{\nabla \bullet D_3 \nabla \phi_3}{D_3 \phi_3} \approx \frac{\nabla \bullet D_2 \nabla \phi_2}{D_2 \phi_2} \approx \frac{\nabla \bullet D_1 \nabla \phi_1}{D_1 \phi_1} = -B^2$$

$$\frac{1}{\phi_3}\frac{\partial \phi_3}{\partial t} \approx \frac{1}{\phi_2}\frac{\partial \phi_2}{\partial t} \approx \frac{1}{\phi_1}\frac{\partial \phi_1}{\partial t} = \tau$$

How good are these assumptions as the gas volume fraction goes from 70% to 95%? For the geometric buckling (i.e. ), the GE lattice code results should provide enough information to estimate the geometric buckling for the three different energy groups. The accuracy of the assumption concerning the time derivative of the group neutron fluxes would seem to depend upon how rapidly the cross sections change with time. For example, if steam volume fraction goes from 70% to 90% in a given region in the BWR core, then the thermal neutron flux in that region would be expected to decrease. If fewer neutrons are slowed down from the fast group, then the fast group neutron flux would increase. However, with fewer thermal neutrons, the fast group source of fast neutrons (i.e. fissions) would tend to decrease. How do errors in assumptions given above affect a typical BWR instability calculation?

**GE Response**

Based on the stated concern regarding the time derivative, the question seems to imply that rapidity of the void fraction (gas volume fraction) change from 70% to 90% will have an impact on the accuracy of the method. This response will clarify that this is not the case. The question also seems to imply that the geometric buckling dominates the nodal reactivities as if the model were a point model. This response will show that the nodal reactivities as a function of time are dominated by the nodal material compositions and the neutron currents between nodes is of secondary importance.

The accuracy of the spatial derivatives depends both on temporal response of the flux gradient and the group diffusion coefficients. It is less obvious that the solution technique also considers indirectly the impact of the changing flux spectrum with time because the flux ratios are reflected in terms of group cross sections via Eqs. 9.1-7 and 9.1-8. It is a common misconception that the modified one-group method cannot account for a changing flux spectrum. This is not true. [[

]] Nearly all the nuclear parameters are sensitive to the moderator density. This dependency is maintained as these parameters are combined into

the parameters defined in 9.1-8 and applied in Eqs. 9.1-9 through 9.1-13. Since this primary dependency on moderator density is modeled, it is essential that the change in moderator density be controlled in order to control the discretization error.

Spatial discretization errors are controlled by choosing an appropriate node size. Even for 100% voids in the channel and 25% voids in the bypass, the diffusion length in the vanished lattice of a typical BWR bundle is less than 3.0 cm, a factor of five smaller than the 15 x 15 x 15 cm cube spatial nodalization. The temporal discretization error is controlled by regulating the time step size to limit the change in the nodal moderator densities that are used to evaluate the nuclear parameters.

The time step size control algorithm documented in Section 8.2.4 of NEDE-32176P, Rev. 2 limits the void fraction change and thus the change in moderator density. As an illustration, consider the calculated results from an extreme regional oscillation where the oscillation amplitude in the most active channel achieves a maximum peak-to-peak over average power ratio of about 3 in about 15 seconds. For this particular example, the period of the oscillation was 1.7 seconds. Of course, the DSS-CD algorithm would have to be disabled to allow the oscillations to ever develop to this extent. Note that the growth rate for this extreme oscillation example is [[ ]], a value that is much larger than what the growth rate limit would allow. Also, note that a scram would occur based on the amplitude of the oscillation. This extreme example was chosen firstly to provide an extreme change in the void fraction over a short period of time and secondly to illustrate how the method is able to accommodate and respond to that rapid change. In this example (see Figure 21-1), the maximum time step size is set to 0.10 seconds so that the only effective control is that provided by the default rate-of-change limits used by the time step control algorithm. The greatest change in the relative water density in the most active bundle occurs in neutronics node 3 about 12% of the way up from the bottom of the core. For this node the maximum recorded change in the relative water density was [[ ]]. The nuclear parameters also experience their greatest change at this time.

Detailed results for neutronics node 13 about half way up the bundle near the end of the fully-rodded section were also extracted for the same lattice so that the values for the nuclear parameters could be combined with those for node 3 to determine their values as a function of void fraction over the void fraction range [[ ]]. Although node 13 is only about mid-height in the core, the peak void fraction during the oscillation is as high as the value at the top of the active fuel in neutronics node 25. The void fraction traces corresponding to neutronics nodes 3, 13 and 25 are shown in Figure 21-2. Note that for this extreme example, the in-channel void fraction is getting as high as [[ ]] in node 13. The DSS-CD algorithm would never allow such a severe case to develop without producing a scram; nevertheless, an ATWS accident scenario could. TRACG has been accepted by the NRC staff as an appropriate tool for calculating ATWS scenarios.

As mentioned previously, the maximum recorded change in the relative water density for node 3 is [[

]] for stability applications used to confirm the DSS-CD algorithm, the time step size will usually be limited to an even smaller value so that the rapidity of the density change is even less of a concern.) The corresponding maximum changes for all the key nuclear parameters also occur at around 12.173 seconds. These maximum changes are provided in column 3 of Table 21-1 along with the corresponding percentage change (column 5) based on the current value (column 4) at the time when the maximum change occurs. The values of the nuclear parameters are also provided in Table 21-1 for the range of void fractions calculated in this extreme example. This information should allow the reviewer to see how the values of the nuclear parameters change as a function of void fraction. All the values are for the lattice in the fully-rodded section of the bundle. The minimum and maximum extent of the void fraction range (in this example) is that experienced at nodes 3 and 13 in the most-active bundle and are the same as the minimum and maximum values shown in Figure 21-1. The change in a nuclear parameter over the full void fraction range is referred to as its *span*. Span is simply the absolute value of the difference between the value in column 9 and the value in column 7. Column 6 of Table 21-1presents the maximum change in the parameter as a percentage of the span in the value. It is useful to present this information in this way because it shows that the %change in the void fraction in terms of its span is related to the %changes in the values of the nuclear parameters relative to their spans. [[

]].

Please notice from the values in Table 21-1 that migration area (FMSQ1) for the fast neutron group is at least a factor of [[ ]] larger than the value for the thermal group for low void fractions near zero and increases to be a factor of [[ ]] as the void fraction approaches one. Similarly, the migration area for group 1 relative to the migration area for the epithermal group is maintained at a relatively constant factor of [[ ]] larger over the entire range of void fractions. The conclusion is that the internodal leakage is dominated by the fast group over the entire range of void fractions. As the void fraction increases and the flux spectrum shifts toward higher energies, the approximation of the flux shape using a single modified group becomes even better. This is because [[

]]. The bucklings for the individual energy groups can be estimated by neglecting the temporal derivative and using the known flux ratios as expressed in terms of the lattice cross sections; however, these simplifications are exactly equivalent to the assumptions used to derive the method, so all they end up producing is the expected result $B_1^2 = B_2^2 = B_3^2 = B^2$. Thus, the justification of the method depends on the two points: [[

]] the approximation of the flux shape using a single modified group becomes better (not worse as postulated).

[[

]] are of secondary importance compared to the nuclear parameters within the node [[

]].

Another aspect of the question is concerned with the impact that the modified one-group assumptions have on typical stability calculations. To address this concern, we will focus entirely on the prediction of the amplitudes and frequencies for the more-challenging regional instability. It is evident from the comparisons of calculated values and data in Sections 7.4 and 7.5 of NEDE-32177P, Rev. 2 that the Leibstadt regional stability tests are a greater challenge than the LaSalle core-wide instability event. Consider the results in Table 21-2 that show how the calculated amplitudes and frequencies from TRACG02, TRACG04 and TRACG05 compare with the data from the Leibstadt stability tests. Note that the TRACG05 model uses [[ ]] whereas the TRACG02 and TRACG04 both use the modified 1-group approximations that are being questioned.

The comparisons in Table 21-2 show that the amplitude/shape separation approximation used in TRACG02 produces essentially the same frequency as [[ ]] TRACG04 and TRACG05. Compared to the TRACG05 [[ ]] solution and most importantly the data, use of the modified one-group approximations has a negligible impact on the ability to predict the frequency for a typical BWR stability event. Thus use of any of the TRACG versions to calculate the frequency of BWR instabilities is appropriate.

Table 21-2 also shows comparisons for the calculated amplitudes. The values of the calculated limit-cycle amplitudes are [[

]]

It is important to remember that the viability of the DSS-CD algorithm does not depend on the ability of TRACG to predict the oscillation amplitude. The viability of the DSS-CD algorithm depends primarily on how well the algorithm preserves CPR margin for a given magnitude of power oscillation. Use of TRACG to assess the viability of the DSS-CD algorithm depends primarily on the fidelity of TRACG in calculating the transient CPR responses for the range of channel power oscillation amplitudes that are expected to occur before the protection system causes a scram. A wide range of power oscillations is possible in the limiting channel [[

]] In other words, concerns with 2% to 5% errors in calculating the rod powers in the lattice physics are all irrelevant. A change of 0.01 to 0.02 in the calculated SLMCPR is also irrelevant in view of the large CPR margin for the DSS-CD algorithm.

Consider a pertinent example related specifically to stability. The peak LPRM amplitude for Leibstadt test 4a predicted by TRACG04 is [[

]]

The best comparisons to ascertain how well TRACG calculates the transient CPR responses are [[

]] Furthermore, instability events do not pose a threat to the integrity of the fuel. In fact, the periodic nature of the flow oscillations ensures that any boiling transition that may occur will be quenched within the period of the

oscillation. So we see that the purpose of the DSS-CD algorithm is to protect the SLMCPR licensing value and has essentially nothing to do with fuel integrity or public safety.

Non-proprietary Version

**Table 21-1 Maximum Change and Span in Values of Nuclear Parameters**

| 1 | 2 | 3 | 4 | 5 | 6 | 7 | 8 | 9 |
|---|---|---|---|---|---|---|---|---|
| **NEDE-32176P, Rev. 2 Symbol** | **Code Name or descriptive name** | **Maximum Change** | **Value at Time of Maximum Change** | **% Change of Current Value** | **% Change of Span in Parameter** | **Parameter Value at Min. Void** | **Parameter Value at 70% Void** | **Parameter Value at Max. Void** |
| $\alpha$ | ALPHA | [[ | | | | | | |
| $u$ | U | | | | | | | |
| $D_1$ | DCOEF1 | | | | | | | |
| $D_2$ | DCOEF2 | | | | | | | |
| $D_3$ | DCOEF3 | | | | | | | |
| $\Sigma_1$ | XR1 | | | | | | | |
| $\Sigma_2$ | XR2 | | | | | | | |
| $\Sigma_3$ | XR3 | | | | | | | |
| $\Sigma_{s\ell 1}$ | XSL1 | | | | | | | |
| $\Sigma_{s\ell 2}$ | XSL2 | | | | | | | |
| $\mu\Sigma_{f1}$ | XNF1 | | | | | | | |
| $\mu\Sigma_{f2}$ | XNF2 | | | | | | | |
| $\mu\Sigma_{f3}$ | XNF3 | | | | | | | |
| $\Sigma_{f1}$ | XF1 | | | | | | | |
| $\Sigma_{f2}$ | XF2 | | | | | | | |
| $\Sigma_{f3}$ | XF3 | | | | | | | |
| Note 1 below | SI2 | | | | | | | |
| Note 2 below | SI3 | | | | | | | |
| $M_1^2$ | FMSQ1 | | | | | | | |
| $M_2^2$ | FMSQ2 | | | | | | | |
| $M_3^2$ | FMSQ3 | | | | | | | |
| Note 3 below | FMEFF | | | | | | | |
| $K_\infty$ | UNKINF | | | | | | | |
| $A_\infty$ | AINFTY | | | | | | | |
| Note 4 | Leakage | | | | | | | |

Non-proprietary Version

| 1 | 2 | 3 | 4 | 5 | 6 | 7 | 8 | 9 |
|---|---|---|---|---|---|---|---|---|
| **NEDE-32176P, Rev. 2 Symbol** | **Code Name or descriptive name** | **Maximum Change** | **Value at Time of Maximum Change** | **% Change of Current Value** | **% Change of Span in Parameter** | **Parameter Value at Min. Void** | **Parameter Value at 70% Void** | **Parameter Value at Max. Void** |
| below | | | | | | | | |
| $B^2$ | B-sqrd | | | | | | | ]] |
| Notes: | | | | | | | | |
| 1 | SI2 | $=\Sigma_{s\ell 1}/\Sigma_2$ | | | | | | |
| 2 | SI3 | $=(\Sigma_{s\ell 1}\Sigma_{s\ell 2})/(\Sigma_2\Sigma_3)$ | | | | | | |
| 3 | FMEFF | $=\left(M^2-A_\infty/\mu_0\right)=\left(M_1^2+M_2^2+M_3^2-A_\infty/\mu_0\right)$ | | | | | | |
| 4 | Leakage | $=\left(M^2-A_\infty/\mu_0\right)B^2$ | | | | | | |

**Table 21-2 Frequency and Amplitude Comparisons for Leibstadt Stability Tests**

[[

| | | | | | | |
|---|---|---|---|---|---|---|
| | | | | | | |
| | | | | | | |
| | | | | | | |
| | | | | | | |
| | | | | | | |
| | | | | | | |
| | | | | | | |
| | | | | | | |
| | | | | | | |
| | | | | | | |
| | | | | | | |
| | | | | | | |
| | | | | | | |
| | | | | | | |
| | | | | | | |
| | | | | | | |
| | | | | | | |
| | | | | | | |
| | | | | | | |
| | | | | | | |
| | | | | | | |
| | | | | | | |
| | | | | | | ]] |

**Figure 21-1, Most-Active Channel Power and Time Step Size**

[[

]]

**Figure 21-2, Void Fractions Near Top, Middle and Bottom of CHAN90**

[[

]]

**Figure 21-3, Effect of Fluid Density on [[**

]]

**NRC RAI 22**

The modified Chisholm correlation given in Report NEDE-32176P, Rev. 2 Eq. 6.2-5, is a function of the flow quality. There is no discussion upon how the flow quality is calculated for evaluation of this correlation. How is the flow quality used in Eq. 6.2-5 calculated? Flow quality is typically calculated based on cell edge velocities and donor cell properties, for example:

$$x_{i+1/2} = \left( \frac{\rho_g \alpha_g v_g}{\rho_g \alpha_g v_g + \rho_f \alpha_f v_f} \right)_{i+1/2}$$

Use of the formula given above for the flow quality to calculate the two-phase frictional multiplier can result in some error for the first cell edge below the Onset of Vapor Generation. The donor cell gas volume fraction for this first cell edge will typically be zero. However, the Onset of Vapor Generation cell will typically have a non-zero void fraction. The TRACG frictional pressure gradient term is for the pressure gradient between cell centers i and i+1. Therefore, an average flow quality between the two half cells from i to i+1/2 and from i+1/2 to i, may be more appropriate for Eq. 6.2-5.

**GE Response**

TRACG solves the mass and energy equations, by solving the mass and energy equations for each cell. Therefore the outflow from each cell minus the inflow is consistent with the energy input to the cell for a steady-state condition. This means that the vapor outflow from a cell as given by:

$$W_{g,i+1/2} = A_{i+1/2} \alpha_i \rho_i v_{g,i+1/2} \qquad \text{for } v_{g,i+1/2} > 0$$

represents the integrated vapor generation up through cell i to the boundary between cell i and cell i+1.

The quality given by

$$x_{i+1/2} = \left( \frac{\alpha \rho_g v_g}{(1-\alpha)\rho_\ell v_\ell + \alpha \rho_g v_g} \right)_{i+1/2}$$

therefore represents the quality at the cell boundary between cell i and i+1. However, the real question is the sensitivity to nodalization. Figure 3.1-6 in the TRACG Qualification LTR (NEDE-32177P, rev. 2) shows the sensitivity in the void profile to the nodalization for a BWR fuel channel. The standard nodalization is [[ ]] nodes. Sensitivity studies were done for [[ ]] nodes. Table 22-1 shows the sensitivity in the pressure drop for the three cases.

These results indicate that the error in the pressure drop due to nodalization sensitivity is approximately [[ ]]. This sensitivity is small compared to the uncertainty in the pressure drop correlations and small compared to the uncertainty that is accounted for in the application methodology as documented in Section 5 of the TRACG Application Methodology LTR [TRACG Application for Anticipated Operational Occurrences transient Analysis, NEDE-32906P-A]

**Table 22-1. Pressure Drop Sensitivity to Nodalization**

| Nodes | [[ | | |
|---|---|---|---|
| Pressure Drop (Pa) | | | ]] |

**NRC RAI 23**

The modified Chisholm correlation for the two-phase frictional multiplier is based on data for flow through 7x7 and 8x8 BWR fuel assemblies. Is there any data comparisons available for 9x9 and 10x10 BWR fuel assemblies for the modified Chisholm correlation? Are there any transient data comparisons for TRACG calculated pressure drop? Is the modified Chisholm correlation used in TRACG components that are representing BWR fuel assemblies (i.e. water rods, jet pumps, steam separators, etc.)?

**GE Response**

Pressure drop comparisons to full-scale data from the ATLAS test facility are made for every fuel product as part of a new product introduction. These comparisons are made using the modified Chisholm correlation for the wall friction and are used to determine the loss coefficients for the spacer pressure drop. For example comparisons for the GE14 10X10 fuel showed that the bundle pressure drop was predicted with a mean error of [[ ]] and a standard deviation of [[ ]].

Comparisons of transient bundle pressure drop are documented in the TRACG Qualification LTR (NEDE-32177P rev. 2). Such comparisons were made for the integral system tests with the TLTA and the FIST test facilities.

The modified Chisholm correlation is used in all TRACG components for the calculation of the wall friction and is used in all TRACG qualification and applications. It is the only correlation that is available in TRACG for wall friction.

**NRC RAI 24**

In report NEDC-33075P, Rev. 3, in Table 5-3, Core Pressure Drop has no Bias and no Deviation applied to and no adjustments for the bounding BWR/6 calculations. It is assumed that this is because the Core Pressure Drop is affected by the Lower Tie Plate Pressure Drop, the Spacer Pressure Drop, and the Upper Tie Plate Pressure Drop which do include Bias and Deviations. For the bounding BWR/6 calculations, only the Spacer Pressure Drop was adjusted. [[

]] Or was spacer loss coefficients for the stable BWR fuel assemblies reduced, while the spacer loss coefficients for the un-stable BWR fuel assemblies increased?

**GE Response**

The Core Pressure has no Bias and had no Deviation applied because the core pressure drop is affected by the lower tie plate pressure drop, the spacer pressure drop, and the upper tie plate pressure drop, which do include bias, and deviations. [[

]]

**NRC RAI 25**

In report NEDE-3217P, Rev. 2, Section 6.1.8, page 6.1-26, Fig. 6.1-5 compares calculated versus measured void fraction for an 8x8 BWR fuel bundle at 6.8 MPa. Are there similar comparisons available for 9x9 and 10x10 BWR fuel bundles?

**GE Response**

The interfacial shear model used for the prediction of void fractions has been qualified against 8X8 bundle data and simple geometry data covering a wide range of hydraulic diameters. The variation in hydraulic diameter between the various BWR fuel product lines is relatively small, ranging from [[ ]] and therefore the void fractions will be very similar for similar fluid qualities. The 8X8 bundle data used in the qualification had a hydraulic diameter of [[ ]]. The smallest hydraulic diameter in the BWR fuel product lines is [[ ]] and is found in the fully rodded section of the 10X10 fuel bundles. There are no available void fraction data for 9X9 and 10X10 bundles, but comparison to simple geometry data for a hydraulic diameter of [[ ]] is shown in Figure 25-1 [density Measurements of Steam-Water Mixtures Flowing in a Tubular Channel Under Adiabatic and heated Conditions, CISE-R-291]. This hydraulic diameter bounds the hydraulic diameter for 10X10 fuel.

Figure 25-1. Comparison to Void fraction Data for $H_D$ = 0.009 m

[[

]]

**NRC RAI 26**

In report NEDC-33075P, Rev. 2, page 5-26, in Table 5-3, the adjustments to the BWR/6 Base Case for the Onset of Vapor Generation is 0.75. The magnitude of this adjustment is based on the uncertainty of +/- 25% for the original Saha-Zuber correlation. If at the onset of vapor generation is reduced by 25%, then onset of vapor generation would move up in the BWR fuel bundle. This implies that the ratio of single phase to two-phase pressure drop would increase. Is this conservative for a typical BWR instability analysis (i.e. larger ratios of single phase to two-phase pressure drop)? Has a TRACG BWR instability calculation been run with a factor of 1.25 for the onset of vapor generation?

**GE Response**

See the response to RAI 27.

**NRC RAI 27**

The uncertainty in subcooled void fraction is assumed to be controlled by the adjustment of two parameters (i.e. interfacial shear distribution parameter – PIRT(22) and subcooling for net vapor generation – PIRT(23)). For subcooled voids, the $C_0$, subcooled boiling varies from 0 to C0:

[[ ]]

A fraction of the wall heat flux goes into flashing water into steam based the Rouhani-Bowring model:

$$q''_{evap} = q''_w \left[ 1 - \left( \frac{h_f - h_\ell}{h_f - h_{\ell d}} \right) \left( 1 + \left( \frac{h_\ell - h_{\ell d}}{h_f - h_\ell} \right) \left( \frac{\varepsilon}{1+\varepsilon} \right) \right) \right]$$

where,

$$\varepsilon = \frac{\rho_f (h_f - h_\ell)}{\rho_g h_{fg}}$$

The third model that effects void fraction in the subcooled boiling regime is the condensation rate. If the condensation rate (i.e. interfacial heat transfer from the liquid phase to the interface) is large enough, then TRACG will not predict any subcooled voids even if . Fig. 6.1-5 on page 6.1-26 of NEDE-32176P, Rev. 2 seems to have a relatively large number of data points along the line for the TRACG void fraction of zero. Could this be an indication that the TRACG condensation rate for subcooled boiling is too larger? What would be a reasonable uncertainty for the TRACG condensation rate for subcooled boiling? What would be the impact of decreasing the TRACG condensation rate by 10-20% on a typical BWR instability analy

Following comments and questions (28-33) are related to J.G.M. Andersen, etal, "TRACG Qualification," NEDE-32177P, Rev. 2, January, 2000.

**GE Response**

The cases that show zero void fraction represents conditions where the calculated liquid enthalpy is less than the enthalpy $h_{ld}$ for onset of net vapor generation as given by the Saha-Zuber correlation. The specific tests where TRACG calculate zero void fraction, but where the data shows small void fractions, are tests 25, 27 and 29. These cases all have very large inlet subcooling $Wc_p\Delta T_\ell$ relative to the bundle power Q. For all of these three cases,

[[ ]]. An example on this is shown in Figure 27-1 for test case 27.

It is seen that TRACG using the Saha-Zuber Model for the onset of net vapor generation accurately predicts the point where there is a significant increase in the void fraction. The data however also shows that small amounts of vapor may form prior to the onset of net vapor generation. This small amount of vapor is most likely bubbles attached to the wall. The cases 25, 27, and 29 are not typical for conditions where BWR instability might occur. For such cases, the inlet subcooling is generally small compared to the bundle power, and the boiling boundary will be very close to the channel inlet. An example of such a case is test 4. The test conditions for test 4 are shown in Table 27-2 and in Figure 27-2. The lowest elevation where void fraction was measured was 1.2 m corresponding to node 8.

The uncertainty in the Saha-Zuber correlation can be bounded by [[ ]] at the $2\sigma$ level. An uncertainty of [[ ]] is typically used for the onset of net vapor generation in TRACG applications [TRACG Application for Anticipated Operational Occurrences Transient Analysis, NEDE-32906P-A]. An uncertainty of a factor of [[ ]] is assumed for the interfacial heat transfer in TRACG applications, i.e., the interfacial heat transfer is reduced by a factor of [[ ]] or increased by a factor of [[ ]] (TRACG Application for Anticipated Operational Occurrences Transient Analysis, NEDE-32906P-A). Figure 27-3 repeats Figure 6.1-5 from NEDE-32176P and shows the sensitivity to factor of [[ ]] on the liquid subcooling (PIRT(23)) for onset of net vapor generation and to a factor of [[ ]] on the interfacial heat transfer (PIRT(32)). It is seen that it does not impact the cases with zero void fraction, but generally lead to an increase in the void fraction by up to [[ ]] for the subcooled boiling cases. Note subcooled boiling typically exists for void fractions up to 40%.

Sensitivity studies have been performed for one of the FRIGG stability tests. A test case with a Pressure of 3MPa and a power of 3.485MW was chosen for the analysis. The results of the sensitivity study are shown in Table 27-3

The uncertainties in the onset of net vapor generation and condensation heat transfer have a small impact on the decay ratio.

**Table 27-1. Test Conditions for Test Cases 25, 27 and 29**

| Test Case | Mass Flow, kg/sec. | Inlet subcooling, K | Bundle Power, MW | $Wc_p\Delta T_\ell / Q$ |
|---|---|---|---|---|
| 25 | [[ | | | |
| 27 | | | | |
| 29 | | | | ]] |

**Table 27-2. Test Conditions for Test Case 4**

| Test Case | Mass Flow, kg/sec. | Inlet subcooling, K | Bundle Power, MW | $Wc_p\Delta T_\ell / Q$ |
|---|---|---|---|---|
| 4 | [[ | | | ]] |

**Table 27-3. Sensitivity Study f or FRIGG Stability Test (3MPa, 3.485MW)**

| Case | Base Case | Onset of Net Vapor Generation | Condensation Heat Transfer |
|---|---|---|---|
| | [[ | | |
| Decay Ratio | | | ]] |

**Figure 27-1. Void Profile for Test 27**

[[

]]

**Figure 27-2. Void Profile for Test 4**

[[

]]

**Figure 27-3, Sensitivity to Onset of Net Vapor Generation – PIRT(23) =1.25 and Sensitivity to Interfacial Heat Transfer – PIRT(32) = 0.5**

[[

]]

**NRC RAI 28**

Table 3.1-1 Mass Flux range is [[ ]] should have been [[ ]]

**GE Response**

The mass flux range as stated in Table 3.1-1 of the TRACG Qualification LTR is incorrect. The mass flux range should have been [[ ]]. This will be corrected in Rev. 3 of the Model Qualification LTR.

**NRC RAI 29**

Data range for comparison of data with TRACG models may not go into high enough void fraction. Is TRACG calculating void fraction larger than 90% for the BWR power oscillations simulated so far?

**GE Response**

The data range for void fraction as shown in Figure 6.1.5 of the TRACG Model Description LTR include void fractions as high as [[ ]]. The additional qualification shown in the response to RAI 25 shows void fractions as high as [[ ]].

**NRC RAI 30**

The FRIGG test used an outlet peak axial power profile. Are there any data comparisons to TRACG for a bottom peaked axial power profile? Bottom peaked axial power profiles move the boiling boundary closer to the inlet. More of the fuel assembly axial length sees non-zero void fractions, with a bottom peaked axial power profile. Is a bottom peaked axial power profile more conservative for BWR power oscillations?

**GE Response**

The FRIGG OF-64 void fraction tests documented in Section 3.1.1 of the TRACG02 Qualification LTR (NEDE-32177P, Rev. 2) used an outlet peaked axial power profile. The FRIGG tests that were used for the stability qualification and documented in Section 3.7 of the TRACG Qualification LTR used a mid peaked axial power shape. The axial power profile for these stability tests is shown in Figure 3.7-3 of the TRACG Qualification LTR. In addition to the FRIGG stability tests, TRACG has also been compared to plant instability events such as the core wide instability at LaSalle and the regional instability at the Leibstadt stability tests. The axial power profile was bottom peaked with the peak power approximately 2 ft from the bottom of the core for both the LaSalle and the Leibstadt events. Thus TRACG has been qualified against stability data for both inlet peaked and mid peaked axial power profiles. Generally bottom peaked axial power profiles tend to be more severe for regional oscillations while mid-peaked axial power profiles tend to be more severe for core wide oscillations.

**NRC RAI 31**

It appears that TRACG is consistently overpredicting the bundle pressure drop as compared to the ATLAS data (See Fig. 3.5-5). Does this indicate a systematic error in the TRACG pressure drop models? In addition, the error seems to be larger at the lower pressure drops. For BWR power oscillations at reduced core flow, the bundle pressure drop may be in this region where the TRACG pressure drop is lower. Does this have a significant impact on the TRACG BWR power oscillations calculations?

**GE Response**

The calculated pressure drop compared to the ATLAS data as reported in the TRACG Qualification LTR (NEDE-31177P, Section 3.5.3) has a mean bias of [[ ]] and a standard deviation of [ ]]. These data shows a comparison of the bundle pressure drop excluding the inlet pressure drop in the side entry orifice. In reanalyzing these events it was discovered that an error was made in interpolating the pressures between two TRACG cells to match the location of the pressure tap in the test facility. When this error was corrected, the mean bias is [[ ]] and the standard deviation is [[ ]]. The revised figures from the TRACG Qualification LTR are shown in Figures 31-1 thru 31-3. The above comparison was made for GE9 fuel. A similar comparison for GE14 fuel gave very similar results, a mean bias of [[ ]] and a standard deviation of [[ ]]. These uncertainties are consistent with the uncertainties that are included in GE's methodologies [Methodology and Uncertainties for Safety Limit MCPR Evaluations, NEDC-32601P-A, TRACG Application for Anticipated Operational Occurrences Transient Analysis, NEDE-32906P-A, DSS-CD TRACG Application, NEDE-33147P]. The TRACG application methodology for DSS-CD [NEDE-33147P] includes a [[ ]] uncertainty for the spacer pressure drop. This uncertainty covers the small bias in the bundle pressure drop comparisons.

**Figure 31-1**
**NEDE-32177P Rev. 2 Figure 3.5-3. ATLAS Bundle Pressure Drop Comparison**
[[

]]

**NEDE-32177P Rev. 2 Figure 3.5-4. ATLAS Bundle Pressure Drop Summary Comparison**

[[

]]

**NEDE-32177P Rev. 2 Figure 3.5-4. Relative Error in ATLAS Bundle Pressure Drop**

[[

]]

**NRC RAI 32**

In the ATLAS test (Sec. 3.6) it was known which rod was the limiting rod and the limiting rod was simulated with a single rod group. During a typical BWR instability calculation is the limiting rod known? Is the limiting rod also simulated with a single rod group?

**GE Response**

The limiting rod is modeled in the TRACG simulation as a single rod group in the hot bundle.
[[

]] Bundle R-factor is a parameter that characterizes the local peaking pattern with respect to the most limiting rod in the bundle, and is used to calculate the steady state CPR in TRACG. [[

]]

**NRC RAI 33**

The GE mitigation methodology is looking for power oscillations with time periods in the range of 0.8 seconds to 4.0 seconds. The transient ATLAS test in Section 3.6 had a period of ~2 seconds. Would the comparisons be significantly different if the period was 0.8 seconds?

**GE Response**

If the time period for the flow oscillation for the test is reduced from 2 to 0.8 seconds, the time period will be reduced relative to the vapor transit time for the bundle. The impact of such a reduction is that the amplitude of the mass flow and quality oscillations at the top of the bundle will be reduced relative to what they would be for the larger time period. As a result the oscillation amplitude for the CPR oscillations at the top of the bundle, where the MCPR occurs, will be reduced. The referenced ATLAS test in Section 3.6 of the TRACG Qualification LTR (NEDE-32177P, Rev. 2) has a power of 5.2 MW and a time period of approximately 2 seconds for the flow oscillation. [[ ]]. A calculation with the same power, average flow and oscillation magnitude, and only the period of the flow oscillation changed to 0.8 second showed [[ ]].

# ENCLOSURE 4

# MFN 05-133

# Responses to DSS-CD TRACG LTR RAIs

# Affidavit

# General Electric Company

# AFFIDAVIT

**I, Bradley J. Erbes,** state as follows:

(1) I am Manager, Systems Engineering Services, General Electric Company ("GE") and have been delegated the function of reviewing the information described in paragraph (2) which is sought to be withheld, and have been authorized to apply for its withholding.

(2) The information sought to be withheld is contained in Enclosures 2 and 3 to GE letter, MFN 05-133, *Responses to DSS-CD TRACG LTR RAIs*, dated November 11, 2005. The proprietary information in Enclosure 2, *Responses to DSS-CD TRACG LTR RAIs,* is delineated by a double underline inside double square brackets. Proprietary figures are identified with double square brackets before and after the object. The proprietary information in Enclosure 3, *Compact Disk - Proprietary*, is the entirety of the files on the compact disk, which carries the notation "GE Proprietary Information. [3]." In each case, the superscript notation[3] refers to Paragraph (3) of this affidavit, which provides the basis for the proprietary determination.

(3) In making this application for withholding of proprietary information of which it is the owner, GE relies upon the exemption from disclosure set forth in the Freedom of Information Act ("FOIA"), 5 USC Sec. 552(b)(4), and the Trade Secrets Act, 18 USC Sec. 1905, and NRC regulations 10 CFR 9.17(a)(4), and 2.390(a)(4) for "trade secrets" (Exemption 4). The material for which exemption from disclosure is here sought also qualify under the narrower definition of "trade secret", within the meanings assigned to those terms for purposes of FOIA Exemption 4 in, respectively, Critical Mass Energy Project v. Nuclear Regulatory Commission, 975F2d871 (DC Cir. 1992), and Public Citizen Health Research Group v. FDA, 704F2d1280 (DC Cir. 1983).

(4) Some examples of categories of information which fit into the definition of proprietary information are:

a. Information that discloses a process, method, or apparatus, including supporting data and analyses, where prevention of its use by General Electric's competitors without license from General Electric constitutes a competitive economic advantage over other companies;

b. Information which, if used by a competitor, would reduce his expenditure of resources or improve his competitive position in the design, manufacture, shipment, installation, assurance of quality, or licensing of a similar product;

c. Information which reveals aspects of past, present, or future General Electric customer-funded development plans and programs, resulting in potential products to General Electric;

d. Information which discloses patentable subject matter for which it may be desirable to obtain patent protection.

The information sought to be withheld is considered to be proprietary for the reasons set forth in paragraphs (4)a., and (4)b, above.

(5) To address 10 CFR 2.390 (b) (4), the information sought to be withheld is being submitted to NRC in confidence. The information is of a sort customarily held in confidence by GE, and is in fact so held. The information sought to be withheld has, to the best of my knowledge and belief, consistently been held in confidence by GE, no public disclosure has been made, and it is not available in public sources. All disclosures to third parties including any required transmittals to NRC, have been made, or must be made, pursuant to regulatory provisions or proprietary agreements which provide for maintenance of the information in confidence. Its initial designation as proprietary information, and the subsequent steps taken to prevent its unauthorized disclosure, are as set forth in paragraphs (6) and (7) following.

(6) Initial approval of proprietary treatment of a document is made by the manager of the originating component, the person most likely to be acquainted with the value and sensitivity of the information in relation to industry knowledge. Access to such documents within GE is limited on a "need to know" basis.

(7) The procedure for approval of external release of such a document typically requires review by the staff manager, project manager, principal scientist or other equivalent authority, by the manager of the cognizant marketing function (or his delegate), and by the Legal Operation, for technical content, competitive effect, and determination of the accuracy of the proprietary designation. Disclosures outside GE are limited to regulatory bodies, customers, and potential customers, and their agents, suppliers, and licensees, and others with a legitimate need for the information, and then only in accordance with appropriate regulatory provisions or proprietary agreements.

(8) The information identified in paragraph (2), above, is classified as proprietary because it contains detailed results of analytical model, methods and processes including computer codes, which GE has developed, and applied to perform stability evaluations using the detection and suppress capability of the confirmation density algorithm for the GE Boiling Water Reactor ("BWR"). GE has developed this TRACG code for over fifteen years, at a cost in excess of three million dollars. The reporting evaluation and interpretations of the results, as they relate to the detection and suppression capability of the confirmation density algorithm for the BWR was achieved as a significant cost in excess of two hundred and fifty thousand dollars to GE.

The development of the evaluation process along with the interpretation and application of the analytical results is derived from the extensive experience database that constitutes a major GE asset.

(9) Public disclosure of the information sought to be withheld is likely to cause substantial harm to GE's competitive position and foreclose or reduce the availability of profit-making opportunities. The information is part of GE's comprehensive BWR safety and technology base, and its commercial value extends beyond the original development cost. The value of the technology base goes beyond the extensive physical database and analytical methodology and includes development of the expertise to determine and apply the appropriate evaluation process. In addition, the technology base includes the value derived from providing analyses done with NRC-approved methods.

The research, development, engineering, analytical and NRC review costs comprise a substantial investment of time and money by GE.

The precise value of the expertise to devise an evaluation process and apply the correct analytical methodology is difficult to quantify, but it clearly is substantial.

GE's competitive advantage will be lost if its competitors are able to use the results of the GE experience to normalize or verify their own process or if they are able to claim an equivalent understanding by demonstrating that they can arrive at the same or similar conclusions.

The value of this information to GE would be lost if the information were disclosed to the public. Making such information available to competitors without their having been required to undertake a similar expenditure of resources would unfairly provide competitors with a windfall, and deprive GE of the opportunity to exercise its competitive advantage to seek an adequate return on its large investment in developing these very valuable analytical tools.

I declare under penalty of perjury that the foregoing affidavit and the matters stated therein are true and correct to the best of my knowledge, information, and belief.

Executed on the 11TH day of NOVEMBER, 2005.

Bradley J. Erbes
General Electric